Mathematical Modeling and Algorithm Application
ISSN: 3006-0842 | Vol. 6, No. 3, 2025

Surface Integrity Change of Ultrasonic Extruded Shaft Parts and Multi-Objective Optimization

Wu Xiong, Zhenyu Liu*

School of Mechanical Engineering, Tianjin University of Technology and Education, Tianjin, 300222, China
* **Corresponding author**: Zhenyu Liu (Email: LiuZY-Tianjin@outlook.com)

Abstract: In the mechanical industry, ultrasonic extrusion processing (UEP) has been developed to improve the surface properties of 304 stainless steel shaft components. Specifically, variations in processing parameters—including spindle speed, feed rate, extrusion depth, and ultrasonic power—significantly influence surface integrity characteristics such as surface roughness, surface hardness, and residual stress. Firstly a four-factor five-level orthogonal experimental design was first implemented to investigate parameter effects. Then the experimental results were analyzed to explore the influence laws of each process parameter on the surface properties.

Keywords: UEP; 304 stainless steel; surface properties; influence laws.

1. Introduction

Shaft components operate under complex working conditions, rendering them susceptible to fatigue damage, wear, and corrosion. Among these failure modes, fatigue failure induced by continuous alternating loads represents a predominant concern [1]. Prolonged exposure to alternating loads initiates surface fatigue cracks, which progressively propagate with accumulated damage [2,3], ultimately resulting in component failure. Consequently, there is an urgent need to enhance material fatigue resistance through surface-strengthening technologies.

UEP is an advanced surface-strengthening technology that synergistically combines static extrusion forces with high-frequency dynamic impact. The process induces controlled plastic deformation through ultrasonic-frequency vibrations superimposed on static pressure, significantly enhancing surface morphology and mechanical properties [4,5]. Compared to conventional extrusion methods, UEP generates a deeper work-hardened layer and higher magnitude residual compressive stresses, thereby improving fatigue resistance, wear resistance, and corrosion resistance [6]. These technical advantages have established UEP as a widely adopted solution for material-surface strengthening applications across the aerospace and automotive sectors [7].

Extensive research by domestic and international scholars has demonstrated the efficacy of UEP in enhancing surface characteristics of metallic materials, including reduced surface roughness, increased hardness, and elevated residual compressive stress. Yao et al. [8] implemented UEP on TC17 titanium alloy and Inconel 718, achieving simultaneous improvements: microhardness increase, residual stress layer depth expansion, and grain size reduction. Wang et al. [9] conducted finite element simulations and experiments on 42CrMo steel's ultrasonic rolling extrusion process based on its constitutive equation. Results demonstrate consistent residual stress distributions between simulations and experiments. Increased static pressure and amplitude enhance residual stress, while higher rotational speed and feed speed reduce it. Zheng et al. [10] propose a hybrid process combining cryogenic minimum quantity lubrication with ultrasonic rolling strengthening, reducing surface roughness from Ra 2.644 μm to 0.055 μm, increasing residual compressive stress from 321 MPa to 657 MPa, and forming a 3.7 mm-deep reinforced layer to enhance blade surface integrity.

To systematically investigate parameter effects on surface roughness in UEP, Cheng et al. [11] demonstrated that applying ultrasonic surface rolling processing technology to a bearing raceway reduced surface roughness (Ra) to approximately 0.16 μm through a "peak-cutting and valley-filling" mechanism. Fan et al. [12] explored the influence of ultrasonic vibration-assisted hole expansion strengthening process on the fatigue property of 7050 aluminum alloy. The hole expansion strengthening experiments were carried out with or without ultrasonic vibration assistance. The results show that after ultrasonic vibration-assisted hole expansion strengthening, the surface roughness of the specimen's hole wall decreases by 67.86%. Chen [13] compared the prediction results of BP neural networks, GA-BP, and MEA-BP through quantitative analysis and found that the MEA-BP model could achieve the optimal surface roughness for bearing rings.

In order to investigate the parameter-hardness relationship in UEP, Wang et al. [14] employed a sequential methodology combining single-factor simulation analysis with RSM. Their approach systematically identified critical parameter interactions and derived optimized parameter combinations for enhanced surface hardness. Zhu [15] experimentally quantified the influence of UEP parameters on the work-hardening degree of bearing rings, determining the parameter set that maximizes surface hardening. The study validated the robustness of this parameter configuration through experimental verification.

In summary, while extensive domestic and international research has focused on individual surface characteristics in UEP, comprehensive analyses of surface integrity during UEP remain comparatively scarce.

2. Experiments of EUP

2.1. Experimental materials

304 stainless steel was selected for this investigation due to its exceptional corrosion resistance and superior machinability. These characteristics make it indispensable for

industrial applications. The alloy's chemical composition is summarized in Table 1, while its physical and mechanical properties are detailed in Table 2. Specimens are cylindrical 304 stainless steel bars (diameter: 20 mm; length: 100 mm) subjected to turning operations. Post-machining characterization revealed an initial surface roughness (Ra) of 2.446 μm, Rockwell S hardness (HRS) of 6.7, and residual stress of -174.56 MPa.

Table 1. Chemical composition of 304 stainless steel (mass fraction)

Chemical composition	Mass fraction
C	0.07
Si	1.0
Ni	8.0-10.0
Mn	2.0
Cr	18.0-20.0
S	0.03
P	0.045

Table 2. Physical and mechanical properties of 304 stainless steel.

Property	Numerical value
Density (g/cm^3)	7.93
Tensile strength (MPa)	520
Yield strength (MPa)	205
Rate of elongation (%)	40
Modulus of elasticity (GPa)	200
Electrical resistivity (10^-6Ωm)	0.73

2.2. Principle of EUP

The core system of UEP comprises two critical subsystems: an ultrasonic generator and a resonant mechanical actuator. The actuator assembly integrates a piezoelectric transducer (PZT-8), alloy horn, and tool tip to achieve controlled surface plastic deformation [错误!未找到引用源。]. Workpieces are securely clamped using a three-jaw hydraulic chuck to ensure vibration stability during processing. The kinematic principles of UEP are illustrated in Figure 1, while the experimental setup is showed in Figure 2.

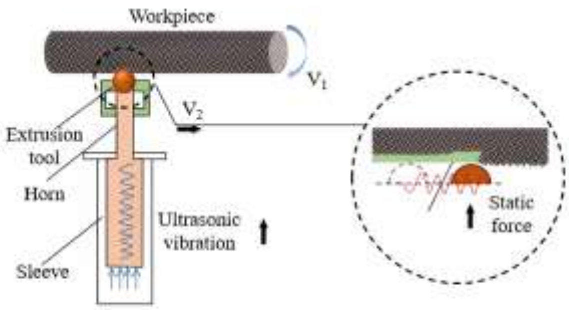

Figure 1 Kinematic principles of UEP.

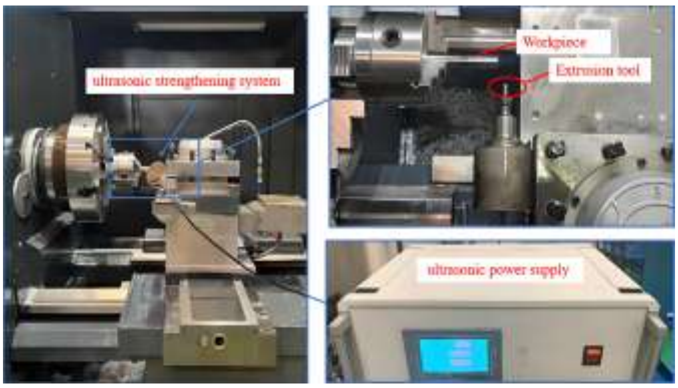

Figure 2 Experimental setup of UEP.

UEP operates through a sequential energy conversion chain:

Electromechanical transduction: The ultrasonic generator converts 50 Hz power into a high-frequency electrical signal.

Piezoelectric conversion: A lead zirconate titanate transducer transforms electrical energy into axial mechanical vibrations.

Mechanical amplification: An alloy horn amplifies vibrations and transmits them to the tool tip.

Surface plasticization: Under controlled pressure, the vibrating tool induces plastic deformation through superimposed static-dynamic loading, generating nanocrystalline surface layers.

2.3. Experimental design and results

Prior to experimentation, specimens underwent uniform machining under identical cutting parameters. A four-factor five-level orthogonal experiment was employed, with full experimental parameter combinations detailed in

Table 3 Key process variables included spindle speed, feed rate, extrusion depth, and ultrasonic power.

Table 3. Experimental design

Factor / Level	Spindle speed (r/min)	Feed rate (mm/r)	Extrusion depth (μm)	Ultrasonic power (W)
1	100	0.01	20	10
2	200	0.04	40	20
3	300	0.07	60	30
4	400	0.10	80	40
5	500	0.13	100	50

Spindle speed selection necessitates a balance between energy input and thermal management effects. At speeds below 100 r/min, insufficient energy density impeded effective plastic deformation and significantly lowered processing efficiency. Conversely, speeds exceeding 500 r/min induce localized heat accumulation, triggering material softening and abnormal tool wear. Thus the spindle speed should be maintained within 100–500 r/min to ensure stable dynamic plastic flow.

Feed rate optimization requires coordination between surface forming quality and deformation compatibility. Below 0.01 mm/r, tool dwell effects cause repeated plastic strain, inducing burr formation. Exceeding 0.13 mm/r results in strain rates surpassing the material's deformation compatibility, generating surface cracks. The optimal feed range of 0.01–0.13 mm/r ensures continuous and uniform deformation.

Extrusion depth directly governs deformation layer depth and machining precision. Depths below 20 μm produce shallow deformation zones insufficient for effective grain refinement, while depths exceeding 100 μm provoke macro-scale material spalling, compromising dimensional stability. Therefore, the 20–100 μm range balances microstructural modification requirements with geometric accuracy control.

Ultrasonic power settings must align with the material's dynamic response characteristics. Power below 10 W generates only elastic deformation, failing to activate dislocation multiplication mechanisms. Overheating above 50 W induces abnormal dynamic recrystallization and microcrack initiation. The 10–50 W range sustains heterogeneous plastic deformation dominance.

The experimental results presented in

Order number	Spindle speed (r/min)	Feed rate (mm/r)	Extrusion depth (μm)	Ultrasonic power (W)	Surface roughness (μm)	Surface hardness (HRS)	Residual pressure (MPa)
	00	0.01	20	10	0.692	7	-1176.78
2	100	0.04	40	20	0.763	8.3	
3	100	0.07	60	30	0.801	8.9	
4	100	0.1	80	40	0.766	9.2	
5	100	0.13	100	50	0.802	8.1	
6	200	0.01	40	30	0.692	10.9	
7	200	0.04	60	40	0.828	11.7	
8	200	0.07	80	50	0.889	11.6	
9	200	0.1	100	10	0.968	13.6	
10	200	0.13	20	20	0.975	8.7	
11	300	0.01	60	50	0.781	10.3	
12	300	0.04	80	10	1.148	13.6	
13	300	0.07	100	20	0.93	15	
14	300	0.1	20	30	0.914	10.4	
15	300	0.13	40	40	1.026	12.3	
16	400	0.01	80	20	0.747	12.6	
17	400	0.04	100	30	0.803	14.7	
18	400	0.07	20	40	0.734	9.4	
19	400	0.1	40	50	0.856	11.6	
20	400	0.13	60	10	0.796	13.8	
21	500	0.01	100	40	0.477	10.6	
22	500	0.04	20	50	0.493	8.3	
23	500	0.07	40	10	0.404	9.5	
24	500	0.1	60	20	0.426	13.9	
25	500	0.13	80	30	0.442	17.2	

demonstrate that UEP significantly enhances the surface characteristics of 304 stainless steel. Specifically, the optimal parameters for minimum surface roughness optimization were achieved at a spindle speed of 500 r/min, a feed rate of 0.07 mm/r, an extrusion depth of 40 μm, and a power of 10W. Maximum surface hardness optimal parameters were obtained with a spindle speed of 500 r/min, a feed rate of 0.13 mm/r, an extrusion depth of 80 μm, and a power of 30W. The maximum compressive stress was attained through a spindle speed of 200 r/min, a feed rate of 0.01 mm/r, an extrusion depth of 40 μm, and a power of 30W.

Table 4. Experimental results

Order number	Spindle speed (r/min)	Feed rate (mm/r)	Extrusion depth (μm)	Ultrasonic power (W)	Surface roughness (μm)	Surface hardness (HRS)	Residual pressure (MPa)
1	100	0.01	20	10	0.692	7	-1176.78
2	100	0.04	40	20	0.763	8.3	-1003.81
3	100	0.07	60	30	0.801	8.9	-980.16
4	100	0.1	80	40	0.766	9.2	-820.01
5	100	0.13	100	50	0.802	8.1	-705.8
6	200	0.01	40	30	0.692	10.9	-1334.27
7	200	0.04	60	40	0.828	11.7	-1078.68
8	200	0.07	80	50	0.889	11.6	-1002.83
9	200	0.1	100	10	0.968	13.6	-1054.23
10	200	0.13	20	20	0.975	8.7	-669.82
11	300	0.01	60	50	0.781	10.3	-1132.68

12	300	0.04	80	10	1.148	13.6	-1089.53
13	300	0.07	100	20	0.93	15	-1132.34
14	300	0.1	20	30	0.914	10.4	-835.4
15	300	0.13	40	40	1.026	12.3	-837.83
16	400	0.01	80	20	0.747	12.6	-1104.55
17	400	0.04	100	30	0.803	14.7	-1043.61
18	400	0.07	20	40	0.734	9.4	-988.37
19	400	0.1	40	50	0.856	11.6	-741.66
20	400	0.13	60	10	0.796	13.8	-939.18
21	500	0.01	100	40	0.477	10.6	-1048.54
22	500	0.04	20	50	0.493	8.3	-1002.8
23	500	0.07	40	10	0.404	9.5	-1068.47
24	500	0.1	60	20	0.426	13.9	-1140.91
25	500	0.13	80	30	0.442	17.2	-1075.32

2.4. Instruments and methods for the material property experiment

The surface roughness measurements were conducted using a JD520 profilometer operating on inductive measurement principles in compliance. The diamond-tipped stylus tip radius traversed the workpiece surface via a motorized linear stage at a constant velocity of 0.5 mm/s, where vertical displacement signals were amplified through a differential transformer, processed via phase-sensitive detection, and digitally integrated to calculate Ra values with 0.01 μm resolution. A sampling length of 0.8 mm and evaluation length of 5.0 mm were implemented, with triplicate circumferential measurements performed at 120° intervals on each workpiece surface to minimize positional bias. The arithmetic mean of three validated measurements was adopted as the final Ra value, ensuring statistical reliability.

The surface hardness of 304 stainless steel specimens was quantitatively evaluated using the Rockwell hardness test in accordance. Specimens were securely mounted on a tungsten carbide anvil, and a diamond conical indenter applied a 150 kgf major load with a 10-second dwell time to generate standardized indentations. Post-test optical microscopy confirmed well-defined indentation geometries without cracking or edge defects. Hardness values were automatically calculated by the HRS-150C Rockwell hardness tester through continuous depth measurement during load transition from preliminary (10 kgf) to total (150 kgf) load states, ensuring elimination of surface finish interference. Triplicate measurements at 2 mm intervals, confirming testing protocol reliability.

Residual stress measurements on 304 stainless steel surfaces were performed using a PROTO /LXRD high-speed X-ray diffractometer. The system configuration included a Cu-Kα radiation source operated at 30 kV and 25 mA, with a 0.5 mm collimator for beam focusing. A fixed ψ-tilt geometry was employed to determine lattice strain distributions. Diffraction patterns were acquired in the 2θ range of 140°-160°, with data analyzed using the Bragg equation and Hooke's law. Stress states were resolved through d-spacing variation analysis, with measurement repeatability verified through triplicate tests.

3. Analysis and discussion of experimental results

3.1. Range analysis of experimental results

Table 5. Range analysis of experimental results

Factors / Level	Spindle speed A (r/min)	Feed rate B (mm/r)	Extrusion depth C (μm)	Ultrasonic power D (W)
k1	0.765	0.678	0.762	0.802
k2	0.870	0.807	0.748	0.768
k3	0.960	0.752	0.726	0.730
k4	0.787	0.786	0.798	0.766
k5	0.448	0.808	0.796	0.764
R of surface roughness	0.512	0.130	0.072	0.072
k1	8.3	10.3	8.8	11.5
k2	11.3	11.3	10.5	11.7
k3	12.3	10.9	11.7	12.4
k4	12.4	11.7	12.8	10.6
k5	11.9	12.0	12.4	10.0
R of surface hardness	4.1	1.7	4.0	2.4
k1	-937.312	-1159.364	-934.634	-1065.638
k2	-1027.966	-1043.686	-997.208	-1010.286
k3	-1005.556	-1034.434	-1054.322	-1053.752
k4	-963.474	-918.442	-1018.448	-954.686

k5	-1067.208	-845.59	-996.904	-917.154
R of surface residual stress	129.896	313.774	119.688	148.484

Range analysis of the orthogonal experimental results was performed to determine the influence of UEP process

Table **5**, where Kij represents the mean value of experimental results for each parameter at level j. The range value Rj, calculated as max {Kij} – min {Kij}, quantifies the variation amplitude of surface roughness when changing the level of factor j. A larger range analysis value (R) indicates a more pronounced impact of the corresponding factor on the index. The range analysis reveals the following order of

Table **5** establishes the parameter influence ranking for surface hardness as A > C > D > B. Maximum surface hardness was recorded at level 4 for parameter A, level 5 for B, level 4 for C, and level 3 for D. This analysis identifies the

Table **5**. Minimum residual stresses were recorded at level 5 for parameter A, level 1 for B, level 3 for C, and level 1 for D. This systematic analysis conclusively identifies the optimal parameter configuration B1D1A5C3 for residual

parameters on surface performance indicators. The corresponding analysis results are presented in
parameter significance for surface roughness: spindle speed (A) > feed rate (B) > extrusion depth (C) > ultrasonic power (D). Minimum roughness values were achieved at level 5 for factor A, level 1 for factor B, level 3 for factor C, and level 3 for factor D. These findings collectively identify the optimal parameter combination A5B1C3D3 for minimal surface roughness.

Range analysis in
optimal parameter configuration A4C4D3 B5 for surface hardness maximization.

The parameter influence ordering for residual stress (B > D > A > C) is presented in

stress minimization.

3.2. The impact of process parameters on surface performance indicators

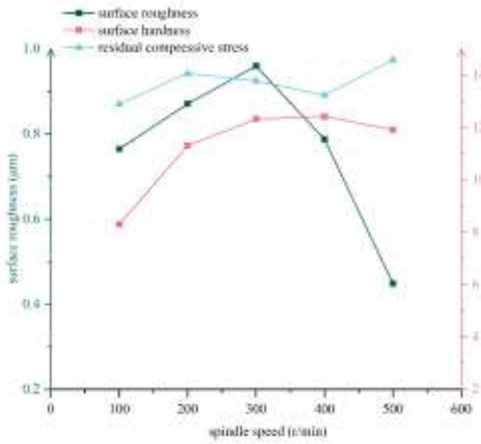

Figure 3. (a) Influence curves of spindle speed on surface performance indicators;

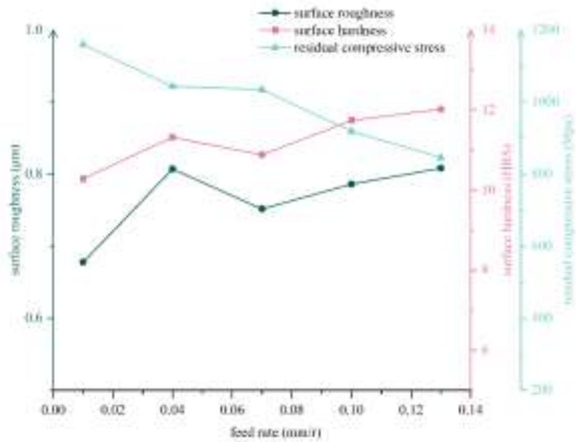

Figure 4. (b) Influence curves of feed rate on surface performance indicators;

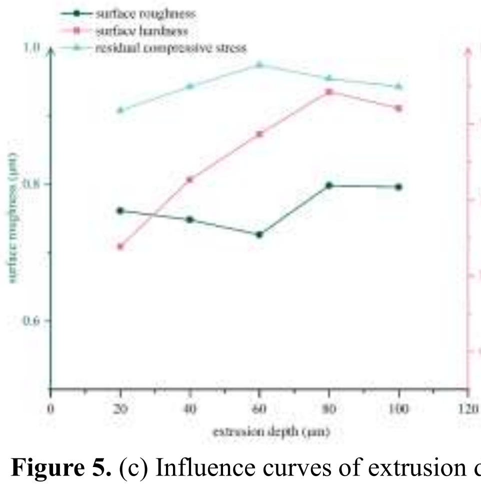

Figure 5. (c) Influence curves of extrusion depth on surface performance indicators;

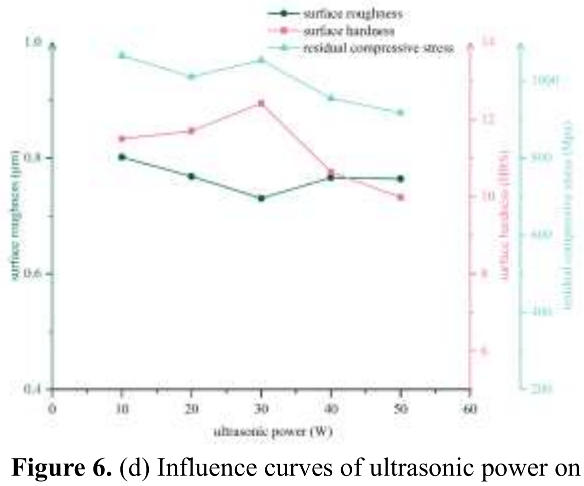

Figure 6. (d) Influence curves of ultrasonic power on surface performance indicators.

The relationship between spindle speed and surface roughness is a non-linear trend, as illustrated in the Figure 3(a). The roughness curve exhibits an initial increase followed by a subsequent decrease with rising rotational speeds. At 300 r/min, surface roughness peaks at 0.960 μm - a remarkable 60.7% reduction compared to the untreated surface. Lower spindle speeds (≤300 r/min) prolong the processing tool's dwell duration at individual surface positions during ultrasonic-enhanced processing. This contact facilitates groove formation through localized plastic deformation, thereby elevating surface roughness. Conversely, higher rotational speeds (>300 r/min) promote dynamic equilibrium between ultrasonic impacts and material flow characteristics. The enhanced kinematic conditions enable more uniform material flow during extrusion, effectively smoothing surface roughness through optimized energy distribution per unit area.

Surface hardness initially increases and then decreases with spindle speed (Figure 3(a)). The hardness peak occurs at 300 r/min, achieving an 85.0% enhancement compared to untreated surfaces. Moderate speeds (100-300 r/min) promote beneficial work hardening through controlled strain accumulation, where dislocations multiply and tangle to strengthen the surface layer [错误!未找到引用源。]. However, excessive speeds (>300 r/min) induce localized over-processing through high-frequency impacts, creating micro-cracks that compromise structural integrity.

As shown in Figure 3(a), it demonstrates a strengthening trend in residual compressive stress with increasing spindle speed. The absolute stress values progress from 937.312 MPa at 100 r/min to 1067.208 MPa at 500 r/min, representing a 13.8% enhancement in compressive stress intensity. This improvement stems from the mechanical energy input per unit area increases, effectively deepening the compressive stress penetration depth.

The surface roughness initially increases, then decreases, and subsequently gradually increases with the increase of the feed rate in the Figure 3(b). This phenomenon arises from the fundamental relationship between feed rate and processing density. Lower feed rates permit complete surface coverage through overlapping ultrasonic impacts, enabling comprehensive asperity flattening. Conversely, higher feed rates create intermittent processing patterns characterized by alternating processed and unprocessed zones along the circumferential surface. This discontinuous treatment generates a mixed surface morphology with increased height differentials between adjacent peaks and valleys, consequently elevating surface roughness.

The response of surface hardness to feed rate variations is revealed in the Figure 3(b). The hardness ascends from 10.3 HRS at 0.01 mm/r to 11.3 HRS at 0.04 mm/r (9.7% increase), then declines to 10.1 HRS at 0.07 mm/r (10.6% reduction), before recovering to 10.8 HRS at 0.13 mm/r. This complex behavior stems from competing deformation mechanisms: Moderate feed rates (0.01-0.04 mm/r) optimize contact duration for effective strain hardening through controlled plastic flow. The higher speeds (0.04-0.07 mm/r) may cause the local surface of the workpiece to be insufficiently extruded, resulting in non-uniform work hardening and a decrease in overall hardness. Excessive speeds (0.04-0.07 mm/r) induce incomplete surface deformation due to reduced tool-workpiece interaction time, creating heterogeneous hardening. Ultra-high rates (0.07-0.13 mm/r) activate dynamic recrystallization effects through accumulated mechanical energy, partially restoring hardness via localized grain refinement.

As depicted in Figure 3(b), when the feed rate increases from 0.01 mm/r to 0.13 mm/r, the residual compressive stress decreases from 1159.364 MPa to 845.59 MPa, as well as the trend shows a significant decrease. The higher feed rate means that the surface of the material is extruded at a faster rate, and the number of extrusions per unit area is reduced, which reduces the overall plastic deformation.

The non-monotonic correlation between extrusion depth and surface roughness is quantified in the Figure 3(c). Minimum roughness values of 0.726 μm (70.3% reduction) occur at 60 μm extrusion depth, relative to the untreated baseline (Ra = 2.446 μm). Controlled parameter selection enables effective roughness reduction. The initial roughness decrease (20-60 μm) corresponds to progressive asperity flattening, where metallic peak material migrates to fill adjacent valleys through controlled plastic deformation. However, exceeding the 60 μm threshold induces scratching from excessive tool-workpiece interaction, reversing surface improvement.

The extrusion depth exhibits a non-linear relationship with hardness, peaking at 80 μm, beyond which excessive deformation reduces material integrity.

When the extrusion depth increased from 20 μm to 60 μm, the absolute value of the residual compressive stress rose from 1054.322 MPa to 1065.638 MPa. However, as the extrusion amount further increased to 80 μm, the absolute residual compressive stress exhibited a declining trend, dropping to 917.154 MPa. At lower extrusion levels, plastic deformation dominates, leading to dislocation accumulation and increased compressive stress. Excessive extrusion may induce surface micro-cracks or grain boundary sliding, diminishing residual compressive stress.

The non-monotonic relationships between ultrasonic power and the three critical parameters — surface roughness, surface hardness, and residual compressive stress — are systematically demonstrated in Figure 3(d). While moderate ultrasonic power (≤30 W) enhances material mobility through optimal energy input, diminishing surface roughness, boosting surface hardness, and uplifting residual compressive stress. Excessive power (>30 W) generates harmful dynamic impacts. These high-energy pulses create localized over-deformation zones that disrupt surface uniformity, ultimately increasing surface roughness, reducing surface hardness, and lowering residual compressive stress.

4. Conclusions

The experimental study yields three principal conclusions. Range analysis methodology identified distinct parameter dominance hierarchies for different surface integrity metrics:

1)Surface roughness: Spindle speed > Feed rate > extrusion depth > Ultrasonic power.

2)Surface hardness: Spindle speed > extrusion depth > Ultrasonic power > Feed rate.

3)Residual stress: Feed rate > Ultrasonic power > Spindle speed > extrusion depth.

References

[1] Zhu, L.; Gong, C.; Zhang, C.; Qian, J.; Liu, S.; Zhang, X.; Liu, C. Robot-assisted ultrasonic impact strengthening strategy for aero-engine blades. Robot. Comput. Integr. Manuf. 2022, 78, 102389. https://doi.org/10.1016/j.rcim.2022.102389.

[2] Duan, C.; Qu, S.; Hu, X.; Jia, S.; Li, X. Microstructures and fatigue behaviors of 25CrNi2MoV steel under electro pulsing-assisted ultrasonic surface rolling. Int. J. Fatigue 2022, 158, 106733. https://doi.org/10.1016/j.ijfatigue.2022.106733.

[3] Pang, Z.; Wang, S.; Yin, X.; Yu, S.; Du, N. Effect of spindle speed during ultrasonic rolling on surface integrity and fatigue

performance of Ti6Al4V alloy. Int. J. Fatigue 2022, 159, 106794. https://doi.org/10.1016/j.ijfatigue.2022.106794.

[4] Wang, Z.; Niu, Y. Effect of ultrasonic vibration extrusion cutting on the corrosion resistance of ultra-fine grained strips. J. Sci. Adv. Mater. Devices 2023, 8(4), 100628. https://doi.org/10.1016/j.jsamd.2023.100628.

[5] Zheng, G.; Luo, X.; Huang, B.; Li, P.; Yang, Y. Distributions of grains and precipitates in gradient lamellae Al–Zn–Mg–Cu alloy by ultrasonic surface rolling processing. Mater. Sci. Eng. A 2021, 825, 141911. https://doi.org/10.1016/j.msea.2021.141911.

[6] Luo, X.; Ren, X.; Jin, Q.; Qu, H.; Hou, H. Microstructural evolution and surface integrity of ultrasonic surface rolling in Ti6Al4V alloy. J. Mater. Res. Technol. 2021, 13, 1586–1598. https://doi.org/10.1016/j.jmrt.2021.05.065.

[7] Zhang, L.; Chen, W.; Wang, X.; Wang, Z. Study on the effect of ultrasonic vibration-assisted compression on mechanical properties and of Ti-45Nb alloy. Mater. Today Commun. 2025, 43, 111641. https://doi.org/10.1016/j.mtcomm.2025.111641.

[8] Yao, C.; Zhou, Z.; Zhao, Y.; Tan, L.; Cui, M.; Wang, Y. Experimental study on surface integrity changes during turning-ultrasonic impact of nickel alloy 718. Int. J. Adv. Manuf. Technol. 2021, 112(5), 1359–1371. https://doi.org/10.1007/s00170-020-06503-3.

[9] Wang, H.; Wang, X.; Tian, Y.; et al. Study on surface residual stress of 42CrMo steel treated by ultrasonic rolling extrusion. Sci. Rep. 2023, 13, 6956. https://doi.org/10.1038/s41598-023-34203-x.

[10] Zheng, Y.; Wu, D.; Wang, H.; Lv, H.; Yu, J.; Liu, X. Formation mechanism of blade surface integrity based on hybrid process of cryogenic minimum quantity lubrication and ultrasonic rolling strengthening process. Mater. Des. 2024, 245, 113235. https://doi.org/10.1016/j.matdes.2024.113235.

[11] Cheng, Y.; Wang, Y.; Wang, Z.; Huang, P.; Zhang, P.; Guo, Q. Ultrasonic surface rolling strengthening and its parameter optimization on bearing raceway. Mater. Des. 2023, 232, 112156. https://doi.org/10.1016/j.matdes.2023.112156.

[12] Fan, Z.; Liu, F.; Su, H.; Xu, J.; Ge, E.; Zhou, E. Ultrasonic vibration assisted hole expansion strengthening of 7050-T7451 aluminum alloy. J. Plast. Eng. 2023, 30(10), 52–59. https://doi.org/10.1016/j.pleng.2023.09.001.

[13] Chen, S.; Zhang, Z.; Xiao, J.; Hu, J.; Zhao, L. Surface roughness prediction of EUP based on MEA-BP neural network. J. Henan Univ. Technol. (Nat. Sci. Ed.) 2021, 40(5), 104–109.

[14] Wang, P.; Wang, X.; Wang, H.; Cheng, L. Finite element analysis and parameter optimization on surface hardness of ultrasonic rolling for 42CrMo steel. Forg. Stamp. Technol. 2023, 48(3), 152–158. https://doi.org/10.13330/j.issn.1000-3940.2023.03.021.

[15] Zhu, Q.; Xu, H.; Wang, X.; Liu, Z.; Long, D. Prediction on degree of work hardening for surface of bearing ring by ultrasonic rolling extrusion based on PSO-BP. Forg. Stamp. Technol. 2021, 46(11), 190–196. https://doi.org/10.13330/j.issn.1000-3940.2021.11.027.